Supporting Information

Simulation of the Cyclic Voltammetric Response of an Outer-Sphere Redox Species with Inclusion of Electrical Double Layer Structure and Ohmic Potential Drop

Katherine J. Levey,[a,b] Martin A. Edwards,[c] Henry S. White,*[d] and Julie V. Macpherson*[a,b]

[a] Department of Chemistry and [b] Centre for Diamond Science and Technology, University of Warwick, Coventry, CV4 7AL, UK

[c] Department of Chemistry & Biochemistry, University of Arkansas, Fayetteville, AR 72701, USA

[d] Department of Chemistry, University of Utah, 315S 1400E, Salt Lake City, UT 84112, USA

*Email - j.macpherson@warwick.ac.uk, white@chemistry.utah.edu

Contents

SI 1. Details of the Finite-Element Model Implemented in COMSOL Multiphysics

Numerical simulations were used to calculate the time- and potential-dependent electric potential, ϕ, and the concentration distribution, C_i of both the supporting electrolyte ions ($i = K^+$ and NO_3^-), and the redox species ($Ru(NH_3)_6^{3+}$ and $Ru(NH_3)_6^{2+}$; $i = O$ and R, respectively) during voltammetry. Mass transport and electric potential are described by the Nernst-Planck and Poisson equations, respectively, eqns (2) and (4) in the main text. We assume that mass transport is by diffusion and migration only i.e. there is no convective transport and no ions can penetrate the compact layer and thus the electric potential within the compact layer is described by the Laplace equation, eqn (3) in the main text.

Electroneutrality of the system is defined by eqn (S1).

$$\sigma_M + \sigma_L = 0$$

where σ_M is the charge density on the metal electrode and σ_L is the charge density in the solution between $x = 0$ and $x = L$ (see eqn. S17 for calculation of σ_L).

The non-faradaic current, i_C, given by eqn (10) in the main text, can be computed from the rate of change of σ_M with time. Equivalently, for voltammetry in which the potential is changed at a constant rate, i_C can also be computed from the rate of change of σ_M with applied potential, E, which is dependent on the scan rate, v, see eqn. (10), 2nd part.

Potential Waveform

The cyclic voltammetry (CV) waveform, $E(t)$, was applied in the COMSOL simulation using piecewise linear functions matching those used in the experiments. Fig. S1 shows an example for a scan rate of 1 V/s. The waveform starts at 0 V vs Ag/AgCl and $E(t)$ is scanned in the positive direction to 0.1 V, swept from 0.1 to -0.5 V and then back to 0.1 V.
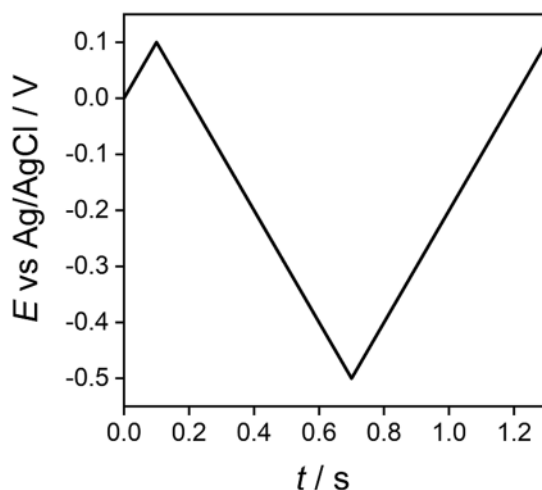
Fig. S1 - *Voltammetric waveform used in both the finite-element simulations and experimental measurements. This example is for a scan rate of 1 V/s.*

Model Parameters

The diffusion coefficient of $Ru(NH_3)_6^{3+}$, $D_{Ru(III)}$, was determined to be $7.5 \pm 0.3 \times 10^{-6}$ cm^2/s from the steady-state voltammetric limiting current, i_{lim}, for reduction of $Ru(NH_3)_6^{3+}$ at a 14.5 ± 0.5 μm radius Pt microdisk electrode (Fig. S2). $D_{Ru(III)}$ was computed from the expression for the diffusion-limited current to a microdisk electrode, $i_{lim} = 4naFD_{Ru\ (III)}C_{Ru(III)}*$, where F is Faraday's constant, $C_{Ru(III)}*$ is the bulk concentration of $Ru(NH_3)_6^{3+}$, and n is the number of electrons transferred per redox species ($n = 1$). The radius, a, was measured using a Leica DM4000M optical microscope. The diffusion coefficient of $Ru(NH_3)_6^{2+}$, $D_{Ru(II)}$, is assumed to be ~1.4 times larger than that of $Ru(NH_3)_6^{3+}$, based on previously reported measurements of this redox couple.[1]
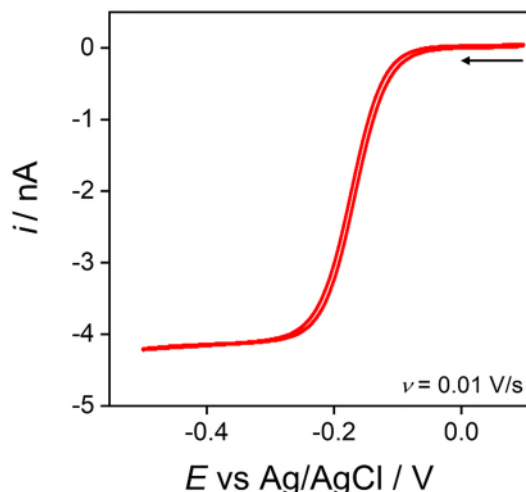
Fig. S2 *Voltammetric response of a Pt microdisk electrode (14.5 ± 0.5 μm radius) in an aqueous solution containing 0.96 mM Ru(NH₃)₆Cl₃ and 1.0 M KNO₃. The solution was bubbled with Ar prior to the measurement to purge dissolved O₂ from the solution. Scan rate = 0.01 V/s.*

Mesh and Accuracy

The Nernst-Planck and Poisson equations were solved for the one-dimensional model shown in Fig. S3. Boundary point 1 (BP1) corresponds to the electrode surface, BP2 to the interface between the inner and outer compact layers ($x = x_1$), BP3 to the outer Helmholtz plane, which we also set as the plane of electron transfer (PET, $x = x_2$), and BP4 to the position of the reference/counter electrode ($x = 2.5$ mm, also equal to the total width of the cell model, L). There are a total of ~350 points in the mesh. The finest mesh elements are near BP3, where the element size is $1/20^{th}$ of the Debye length (κ^{-1} ~0.3 nm in 1.0 M KNO₃, calculated from the reciprocal of eqn (S2)), growing at 5% per element.

$$\kappa = \left(\frac{F^2 \sum_i z_i^2 C_i^*}{\varepsilon_S \varepsilon_0 RT} \right)^{1/2}$$

In eqn (S2), κ is the reciprocal Debye length (m⁻¹), z_i and C_i^* are the charge and the bulk concentration (mol/m³) of species i respectively. R is the ideal gas constant (J mol⁻¹ K⁻¹), T ($= 293.15$ K for all simulations in this work) is the temperature, ε_S is the dielectric constant of water (~80 at $T = 293.15$ K[3]), and F is Faraday's constant (96,485 C mol⁻¹). In the bulk solution between BP3 and BP4, the mesh grows coarser with the maximum element size being $1/50^{th}$ of

the total width of the model ($L = 2.5$ mm). The equations were discretised using linear Lagrange elements.
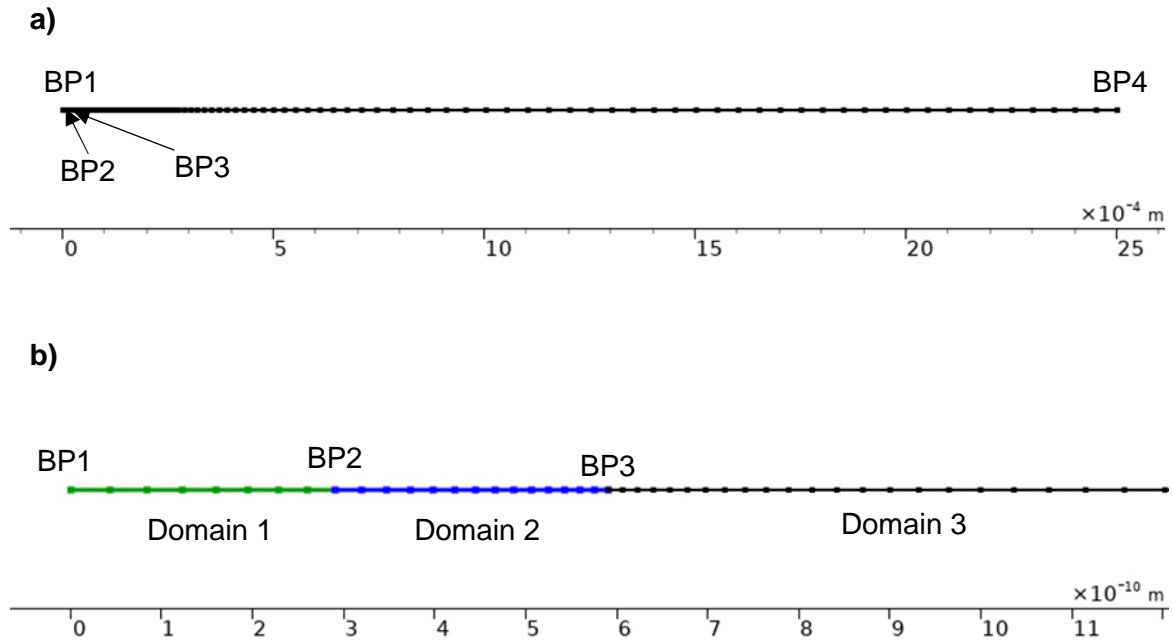
a)

b)

Fig. S3 Geometry and mesh used for finite-element simulations: a) the whole model (2.5 mm), and b) zoomed-in section of the compact layer-electrolyte interface (~1 nm). The green region corresponds to the 0.29 nm thick inner compact layer, the blue region corresponds to the 0.30 nm thick outer compact layer, while the remaining region (black, 0.59 nm < x ≤ 2.5 mm) corresponds to the electrolyte solution.

The accuracy of the simulations was confirmed by performing simulations with progressively finer meshes and comparing the results. We deemed the simulations to be sufficiently accurate when no appreciable changes were observed in the simulated results when using finer mesh elements or higher solver tolerances (as is the case with the mesh described above).

Initial and Boundary Conditions

The initial concentrations ($t = 0$ s) of each species within the electrolyte solution (domain 3; $x > x_2$) were set to match those in the experiments as follows:

$$C_{Ru(III)}(x,0) = C_{Ru(III)}^{*}$$

$$C_{Ru(II)}(x,0) = 0$$

$$C_{K^+}(x,0) = C_{elec}$$

$$C_{NO_3^-}(x,0) = C_{elec} + 3C_{Ru(III)}{}^*$$

where $C_{Ru(III)}$ is the concentration of the oxidised $Ru(NH_3)_6{}^{3+}$ species, $C_{Ru(II)}$ is the concentration of the reduced $Ru(NH_3)_6{}^{2+}$ species, $C_{Ru(III)}{}^*$ is the initial/bulk concentration of the oxidised species and C_{elec} is the initial/bulk concentration of 1:1 supporting electrolyte. NB: the $3C_{Ru(III)}{}^*$ in eqn (S6) represents the contribution of the counterion in the $Ru(NH_3)Cl_3$ salt. For simplicity we assume this to be a NO_3^- salt, instead of adding a second non-electroactive anion species, Cl^- to the simulation.

At the PET (BP3), electron transfer is modelled using Butler-Volmer kinetics, as described by eqns (6) and (7) in the main article. Mass conservation requires:

$$-J_{Ru(III)} = J_{Ru(II)}$$

where J_i is the flux normal to the electrode surface at BP3.

The supporting electrolyte ions (K^+ and NO_3^-), are not consumed in the reaction. Thus, at BP3

$$0 = J_{K^+} = J_{NO_3^-}$$

At BP4 ($x = L$), which represents the location of the reference/counter electrode in bulk solution, the species concentrations were fixed to their bulk values:

$$C_{Ru(III)}(L,t) = C_{Ru(III)}{}^*$$

$$C_{Ru(II)}(L,t) = 0$$

$$C_{K^+}(L,t) = C_{elec}$$

$$C_{NO_3^-}(L,t) = C_{elec} + 3C_{Ru(III)}{}^*$$

The electric potential on BP4 was set to $\phi = 0$ V, while the potential at BP1 was swept by setting $\phi = E(t)$. The CV waveform starts at $E = 0$ V, which is equal to the potential of zero charge, pzc, and is positive of E^0 for the reduction of $Ru(NH_3)_6{}^{3+}$. Thus, at $t = 0$, no electric double layer (EDL) exists, and no redox reaction is occurring. For these initial conditions, the electric potential throughout the domain is given by:

$$\phi(x,0) = 0 \text{ V}$$

The electric potential at the internal boundaries between the inner Helmholtz, outer Helmholtz and solution phases have zero charge, satisfying continuity in ϕ and:

$$\varepsilon_0 \varepsilon_A \frac{d\phi_A}{dx} = \varepsilon_0 \varepsilon_B \frac{d\phi_B}{dx}$$

where the subscripts A and B indicate the phase in which the quantity is evaluated.

Calculating Current Density

The total current density (j_T) was calculated from the sum of the faradaic current (j_F) and non-faradaic charging current (j_C). The faradaic current density was calculated from the flux normal to the electrode (mol m^{-2} s^{-1}) of Ru(NH$_3$)$_6^{3+}$ at the PET (BP3) by eqn (S15).

$$j_F = -nFJ_{Ru(III)}$$

The non-faradaic current density is defined as the rate of change of the charge density at the metal electrode (BP1) with time, eqn (S16), and is evaluated at $x = 0$ on the inner compact layer side of the interface.

$$j_C = \frac{\partial \sigma_M}{\partial t} = \frac{\partial}{\partial t}\left(-\varepsilon_0 \varepsilon_1 \frac{\partial \phi}{\partial x}\bigg|_{x=0^+}\right)$$

Under equilibrium conditions with no electron transfer and at a constant applied potential, the solution to the Poisson-Nernst-Planck equations is equivalent to the analytical Gouy-Chapman-Stern (GCS) model, which can be used to check the accuracy of the numerical calculations. At slow scan rates, the Poisson Nernst-Planck equations solved by numerical simulations are in excellent agreement with the charging currents based on the capacitance computed from the GCS model (data not shown).

The GCS model describes the electric potential and ion concentration distributions across the solution and the surface charge density on the metal electrode, eqn (10) of the main article, and the electrolyte solution, σ_L, eqn (S17). Eqn (S17) is derived from the equilibrium solution to the Poisson-Nernst-Planck equations,[2]

$$\sigma_L = -\left(2\varepsilon_S \varepsilon_0 RT \sum_i C_i^*\left[\exp\left(-\frac{z_i F(\phi_{PET} - \phi_L)}{RT}\right) - 1\right]\right)^{1/2}$$

with C_i^* having units of mol/m^3.

Computational software and hardware

Numerical simulations were formulated using COMSOL Multiphysics 5.6™ (COMSOL, Sweden) using the Chemical Reaction Engineering Module. The simulations were run on HP EliteDesk 800 desktop computer equipped with 64 GB RAM. They took ~ 1 minute per voltammogram to run with 1 mV sampling.

COMSOL model report

To aid in reproducing the simulations described above, an automatically generated COMSOL 'Model Report' is included as a Supplementary Information file for (a) the electrostatic model and (b) the electrostatic model with ohmic potential drop compensation.

SI 2. The Influence of the Potential of Zero Charge on the CV Response

The experiments corresponding to our simulations shown in the main article used a 2-mm diameter polycrystalline Au disk electrode instead of a single crystal. The *pzc* of gold is dependent on the crystallographic orientation.[4] Consequently, the surface of the polycrystalline Au electrode will expose microcrystals with different *pzc* values. In the main text, we assume $pzc = \phi_{\text{ref}} = 0$ V for all simulations. To evaluate the impact of this assumption on our simulations, the formal potential ($E^{0'}$) was varied from -0.2 V to 0.2 V vs ϕ_{ref} (= *pzc*), while the potential window was maintained at $E^{0'} \pm 0.3$ V (this is equivalent to varying the *pzc* while maintaining $E^{0'}$). The results of these simulations are shown in Fig. S4. All other parameters are as stated in the caption to Fig. 2 in the main text, with $k^0 = 13.5$ cm/s. As can be seen in Fig. S4a, the voltammetric response simulations at 1 V/s are independent of *pzc* - $E^{0'}$, with curves for all five *pzc* values overlaying. However, the local concentrations of oxidised (solid) and reduced (dashed) species are strongly dependent on *pzc* - $E^{0'}$, as can be seen in Fig. S4b, which plots their concentrations at the PET as a function of potential vs $E^{0'}$.

First we compare the extreme cases considered, $E^{0'} = +0.2$ V (purple) and $E^{0'} = -0.2$ V (black), in which the potential is positive of the *pzc* for $E - E^{0'} > -0.2$ and > 0.2 V, respectively, to the diffusion only case (black curves Fig. 2c, main text). We see that for potentials negative of the *pzc* the local concentrations of both species are higher than those predicted in the diffusion model due to the positively charged redox couple (both forms) attracted to the negative charge on the metal electrode. At potentials positive of the *pzc*, the reverse is true, both redox species are depleted near the PET. Note, far negative of $E^{0'}$ the oxidised form is difficult to resolve on this plot, due to its rapid reduction, yet in this region, its concentration is also enhanced vs the diffusion model when $E < pzc$ and diminished when $E > pzc$.

The potential drop across the compact layer ($\phi_{\text{M}} - \phi_{\text{PET}}$) vs $E - E^{0'}$ for different *pzc* - $E^{0'}$ is plotted in Fig. S4c. At $E - E^{0'} = pzc$ there is no charge on the electrode, no electric field in the compact layer, and $\phi_{\text{M}} - \phi_{\text{PET}} = 0$ (dashed line). At potentials positive of the *pzc* we see $\phi_{\text{M}} - \phi_{\text{PET}} > 0$ V, indicating a positive charge on the metal and a positive electric field $\left(-\dfrac{\partial \phi}{\partial x}\bigg|_{x=0^+} > 0 \right)$ in the compact layer, while at potentials negative of *pzc*, the reverse is true.
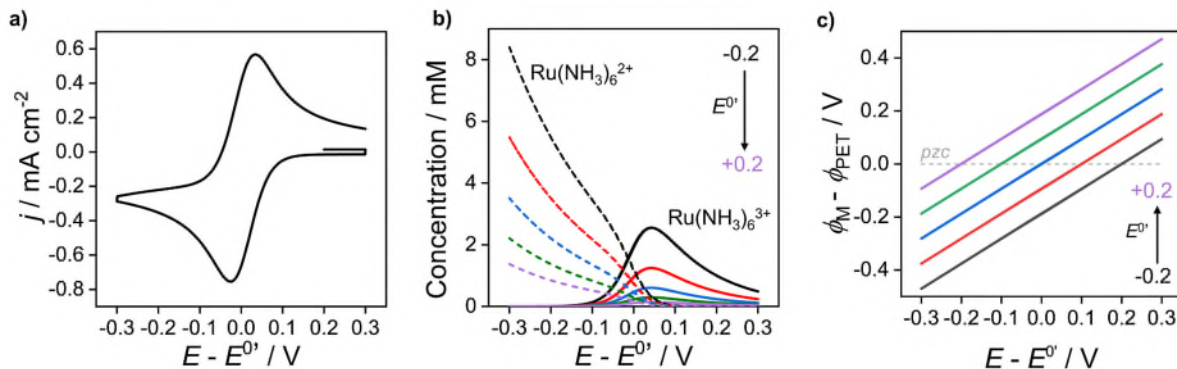
Fig. S4 The simulated a) voltammetric response of 1.0 mM Ru(NH₃)₆³⁺ in 1.0 M KNO₃ when $E^{0'}$ is set at -0.2 V (black), -0.1 (red), 0 V (blue), 0.1 V (green), and 0.2 V (purple). Simulation parameters: $x_1 = 0.29$ nm, $x_2 = 0.59$ nm, $\varepsilon_1 = 6$, $\varepsilon_2 = 30$, $\varepsilon_s = 80$ from reference 3 and 5, $D_{Ru(III)} = 7.5 \times 10^{-6}$ cm²/s and $D_{Ru(II)} = 10.4 \times 10^{-6}$ cm²/s, $k^0 = 13.5$ cm/s, $\alpha = 0.45$, $v = 1$ V/s, and $T = 293.15$ K.[6] (b) Simulated concentrations of Ru(NH₃)₆²⁺ (dashed) and Ru(NH₃)₆³⁺ (solid) at the PET and (c) simulated potential drop across the compact layer ($\phi_M - \phi_{PET}$) as shown by the solid curves. NB: in part (a) all curves overlay and only the black curve is visible.

As shown in Fig. S5, when the electron-transfer kinetics are slowed to quasi-reversible conditions, e.g. $k^0 = 0.1$ cm/s at $v = 1$ V/s, the voltammetric response depends on pzc - $E^{0'}$. The voltammetric response is no longer independent of the structure of the EDL and the local concentration of the redox species. The peak-to-peak separation (ΔE_p) increases from 62 mV when $E^{0'} = -0.2$ V to 86 mV when $E^{0'} = +0.2$ V.

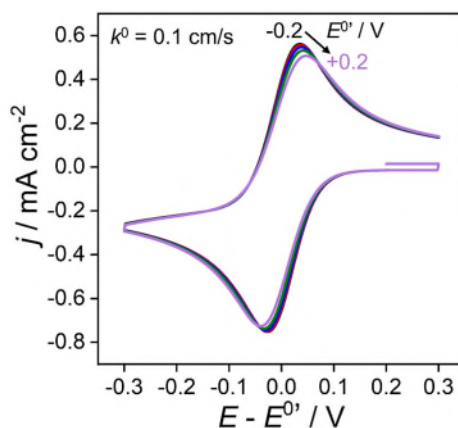**Fig. S5** The simulated voltammetric response of 1.0 mM Ru(NH₃)₆³⁺ in 1.0 M KNO₃ with quasi-reversible electron transfer kinetics ($k^0 = 0.1$ cm/s, $v = 1$ V/s) for pzc = 0 V and $E^{0'}$ set at: -0.2 V (black), -0.1 (red), 0 V (blue), 0.1 V (green), and 0.2 V (purple). All other simulation parameters are as listed in Fig. S4.

SI 3. Determining the Contribution of Electron-Transfer Kinetics to Peak Splitting Using the Diffusion Model

The diffusion model assumes that all the applied potential is dropped across the compact layer (i.e. $E = (\phi_M - \phi_{PET})$ and $\phi_{PET} = 0$ V), and that mass transport occurs only by diffusion. Fig. S6 shows a voltammogram simulated using the diffusion model with $k^0 = 13.5$ cm/s (as used throughout the main text). As shown, the voltammetric response is reversible (i.e. $\Delta E_p = 2.218RT/nF = 56$ mV when $T = 293.15$ K) for $v \leq 100$ V/s and there is no capacitive contribution due to the absence of electrostatics in the model. At 1000 V/s, ΔE_p increases minimally to 59 mV, reflecting a small impact of the electron-transfer kinetics on ΔE_p at these scan rates. This result confirms the claims made in the main text that essentially all the peak splitting observed in the electrostatic model (when $k^0 = 13.5$ cm/s) is due to effects other than the finite electron-transfer kinetics.
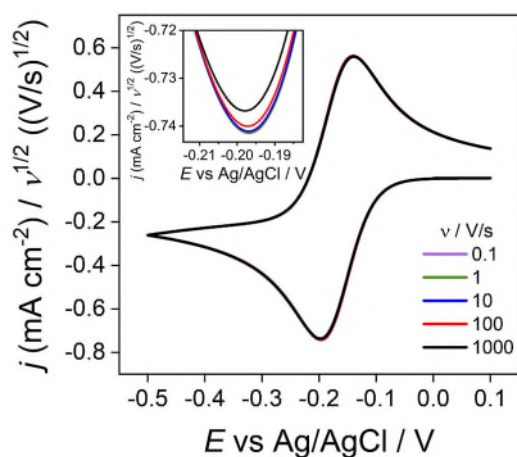

Fig. S6 *The simulated voltammetric response of 1.0 mM $Ru(NH_3)_6^{3+}$ in 1.0 M KNO_3 assuming diffusional transport and no EDL. Literature values of $k^0 = 13.5$ cm/s and $\alpha = 0.45$ were employed.[6] Scan rate, v, as in legend. The current density has been normalised by $v^{1/2}$. Inset: zoomed-in cathodic peak.*

SI 4. Analytical Solution for the Nernstian Concentration of Redox Species at the PET

We provided analytical expressions in the main text, eqns (13) and (14), that describe the concentrations of the redox species at the PET for a reversible electron-transfer reaction. Below, we provide the derivation of these expressions written in terms of O and R.

We assume that mass transport is only by diffusion. The diffusional fluxes of O and R to the PET are as follows:

$$J_R\big|_{x=PET} = -D_R \frac{\partial C_R}{\partial x}\bigg|_{x=PET} = D_R \frac{C_R(x=PET)}{\delta_R(t)}$$

$$J_O\big|_{x=PET} = -D_O \frac{\partial C_O}{\partial x}\bigg|_{x=PET} = -D_O \frac{C_O^* - C_O(x=PET)}{\delta_R(t)}$$

where $\delta_i(t)$ is the time-dependent diffusion layer thickness of species i.

For planar diffusion, $\delta_i(t)$ is described by eqn (S20)

$$\delta_i(t) = (2D_i t)^{1/2}$$

Substitution of eqn (S20) into eqns (S18) and (S19), yields:

$$J_R\big|_{x=PET} = \frac{D_R}{(2t)^{1/2}}\left(C_R(x=PET)\right)$$

$$J_O\big|_{x=PET} = -\frac{D_O}{(2t)^{1/2}}\left(C_O^* - C_O(x=PET)\right)$$

Mass conservation at the PET requires:

$$J_O\big|_{x=PET} = -J_R\big|_{x=PET}$$

Substituting eqns (S21) and (S22) into eqn (S23) yields eqn (S24)

$$\frac{D_O^{1/2}}{(2t)^{1/2}}\left(C_O^* - C_O(x=PET)\right) = \frac{D_R^{1/2}}{(2t)^{1/2}}\left(C_R(x=PET)\right)$$

which can be rearranged to obtain the concentration of C_R at the PET in terms of C_O and C_O^*

$$C_R(x=PET) = \frac{D_O^{1/2}}{D_R^{1/2}}\left(C_O^* - C_O(x=PET)\right)$$

Combining eqn S25 with the Nernst equation (eqn S26)

$$E = E^{0'} + \frac{RT}{nF}\ln\frac{C_O(x=\text{PET})}{C_R(x=\text{PET})}$$

yields the potential dependence of C_O at the PET, eqn (S27). This solution is substituted into the Nernst equation to determine the potential dependence of C_R at the PET, eqn (S28).

$$C_O\left(x=\text{PET}\right) = \frac{\left(D_O^{1/2}/D_R^{1/2}\right)C_O^{*}\exp(\xi)}{1+\left(D_O^{1/2}/D_R^{1/2}\right)\exp(\xi)}$$

$$C_R\left(x=\text{PET}\right) = \frac{\left(D_O^{1/2}/D_R^{1/2}\right)C_O^{*}}{1+\left(D_O^{1/2}/D_R^{1/2}\right)\exp(\xi)}$$

where $\xi = \frac{nF}{RT}\left(E-E^{0'}\right)$. Eqns (S27) and (S28) are equivalent to eqns (13) and (14) in the main text.

SI 5. Experimental and Simulated Voltammetric Background Responses in 1.0 M KNO₃

In simulations where only supporting electrolyte is present in the solution, the background charging current response, outside of the switching regions, overlay (within the width of a line on the scale shown) when normalised by scan rate and area to give the capacitance density (μF/cm^2) of the electrode material. This is shown in Fig. S7a using the electrostatic model for a 2-mm diameter polycrystalline Au disk electrode in 1.0 M KNO₃ solution. Whilst the time constant controlling the current decay, following potential switching at 0.1 V and -0.5 V, is constant, the current decay is more visible as the time scale of the scan decreases with increasing scan rate. Note, the normalised responses for experiments recorded in 1.0 M KNO₃ using a 2-mm diameter polycrystalline Au disk electrode ($A = 0.0314$ cm^2) do not overlay, Fig. S7b, and exhibit a sloping background. We attribute these non-ideal features to leakage of the electrolyte between the Kel-F$^®$ insulator shroud and Au electrode. The consequence of a non-perfect electrode-insulator seal becomes more pronounced at slower scan rates.[2]
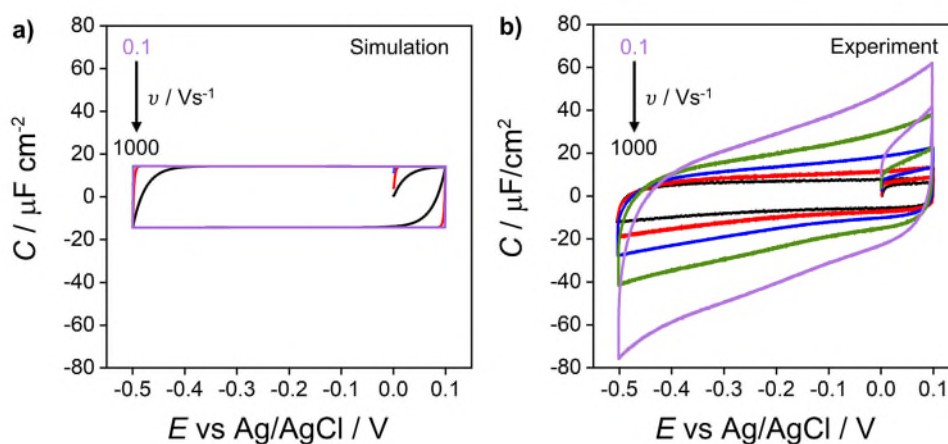

Fig. S7 *a) Simulated and b) experimental voltammetric responses of a 2-mm diameter polycrystalline Au disk electrode in 1.0 M KNO₃ at varying scan rates (normalised to give capacitance density). All other parameters are as listed in the caption of Fig. 2 in the main article*

SI 6. Simulating Positive Feedback Ohmic drop Compensation

Uncompensated resistance between the working electrode and the reference electrode ($x = L = 2.5$ mm) impacts the voltammetric response through the ohmic potential drop, which occurs from just outside of the EDL to the reference electrode (ϕ_L). Potentiostats typically possess the functionality to adjust the applied potential to compensate for the majority of the ohmic potential drop, such that the potential difference between the working electrode and the solution, just outside the EDL, is close to the time-dependent applied potential, $E(t)$. The section below describes how ohmic potential drop compensation is included in our simulations, the results of which are presented in Fig. 5 of the main text. A COMSOL model report that includes ohmic potential drop compensation is provided as an additional Supplementary Information file.

While the precise implementation of ohmic drop compensation in potentiostats depends on the electronic circuitry used, it is typically achieved through a positive feedback loop. Ohmic drop is continually estimated by multiplying the measured current (i) by the solution resistance (R_u). The feedback loop adjusts the applied potential by a proportion (e.g. 95%) of this estimated ohmic potential drop. These adjustments aim to maintain the potential difference between the reference and working electrode by applying the compensated potential difference, $E_{comp}(t) \sim E(t) + (iR_u \times f)$. Where f the fraction of the iR_u drop added back to the applied potential (the approximate sign indicates that $E_{comp}(t)$ depends on the response time of the feedback loop). In a similar way to a potentiostat using a positive feedback loop, we include ohmic potential drop compensation within numerical simulations. Initially, we calculate the bulk conductivity (γ) of the electrolyte solution:

$$\gamma = F \sum |z_i| u_i C_i$$

where z_i is the charge, u_i is the mobility and, C_i is the bulk concentration of species i. The mobility of the ions in solution is calculated using the Nernst-Einstein relation:

$$u_i = \frac{|z_i| F D_i}{RT}$$

The solution resistance (R_u) is calculated as

$$R_u = \frac{L}{\gamma A}$$

where A is the electrode area and L is the width of the cell, 2.5 mm. Note, in this calculation, we implicitly assume that the solution conductivity remains at its bulk value and that the electrode reaction does not alter this conductivity. This is generally true, except within the EDL. However, since the thickness of the EDL is typically orders of magnitude smaller than 2.5 mm, it does not significantly contribute to the overall solution resistance.

For C_{elec} = 1.0 M, L = 2.5 mm, T = 293.15 K, D_{K^+} = 2.0×10^{-5} cm^2/s and $D_{NO_3^-}$ = 1.9×10^{-5} cm^2/s), γ and R_u are computed, respectively to be 14.9 S/cm (including K$^+$, NO$_3^-$ and Ru(NH$_3$)$_6$$^{3+}$) and R_u = (1.67×10^{-4}) Ωm^2/A, where A is the electrode area that defines the cross-section area of the prismatic rectangular cell that current passes through.

To mimic the feedback loop we introduce a differential equation which tracks the ohmic drop through the variable ρ

$$\frac{d\rho}{dt} = k\left(R_u i - \rho\right)$$

where k (a positive number, units s^{-1}) is the gain parameter of the feedback loop which alters how quickly the feedback loop responds to changes in current. The initial value of ρ is set to 0 V. Substituting eqn (S31) and the current ($i = (j_C + j_F)A$) into eqn (S32) gives

$$\frac{d\rho}{dt} = k\left(\frac{1}{\gamma A}\left(j_C + j_F\right)A - \rho\right)$$

$$= k\left(\frac{1}{\gamma}\left(j_C + j_F\right) - \rho\right)$$

where we observe that the electrode area (A) is eliminated, meaning that the expression is universal to planar electrodes represented by Fig. S3.

E_{comp} is described by

$$E_{comp}(t) = E(t) + \rho \times f$$

It is applied as the potential on BP1 and is used as the electrode potential in the Butler-Volmer expression for electron transfer kinetics, eqns (6) and (7).

Fig. S8 compares the response when using 95% (f = 0.95) ohmic potential drop compensation (red lines) with that when no compensation is applied (black lines). From the voltammograms shown in Fig. S8a we have selected potential values from the negatively and positively scanning

sweeps corresponding to I) $E = -0.200$ V (negative direction) and II) $E = -0.150$ V (positive direction) respectively. The electric potential distribution across the domain (insets show potential within 3 nm of the electrode surface) with and without ohmic potential drop compensation are shown in Fig. 8b at $E = -0.200$ V and in Fig. 8c at $E = -0.150$ V.
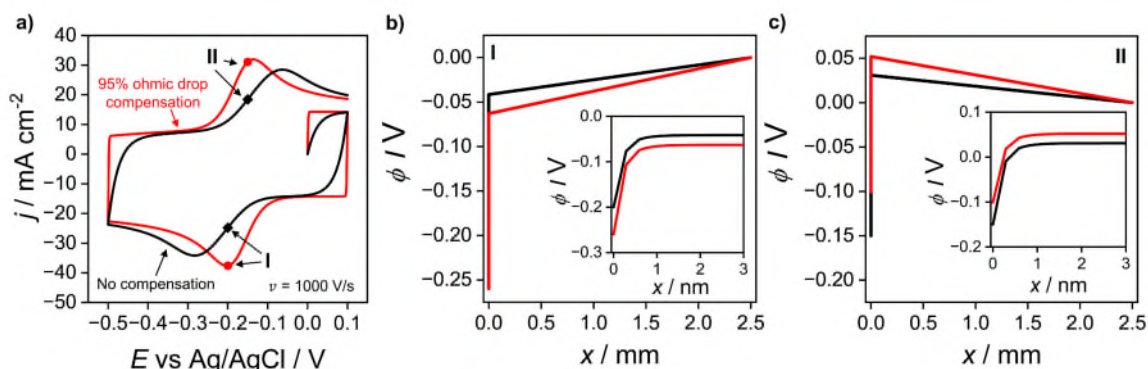

Fig. S8 *a) CVs without (black) and with (red) 95% ohmic drop compensation at a scan rate of 1000 V/s. Simulated electric potential distribution across the cell (inset: within 3 nm of the electrode) at b) E = - 0.2 V (cathodic) and c) E = -0.15 V (anodic) as labelled on part a respectively as I and II. All other parameters are as listed in the caption to Fig. S4. The curves in (a) are reproduced from Fig. 5a and b in the main text.*

In Fig. S8b the uncorrected potential applied to the electrode during the negative scanning portion of the CV is -0.200 V vs the reference electrode potential (= 0 V), black line. The value of ϕ at the electrode surface ($x = 0$) is shown more clearly in the inset. However, the potential difference between the solution just outside the EDL (~ -0.042 V) and the metal (-0.200 V) is only ~ -0.158 V, which reflects the potential difference the electrode experiences when accounting for ohmic potential drop. In contrast the red line data shows that to account for the ohmic potential drop, the electrode must experience a corrected potential (red line) of -0.260 V vs the reference electrode potential. The potential difference between the solution just outside the EDL (~ -0.063 V) and the metal (-0.260 V) is now ~ -0.200 V.

Fig. S8c shows the potential distribution from the positively scanning portion of the CV where the uncorrected potential is -0.150 V vs the reference electrode potential (black line), whilst the corrected potential is ~ -0.100 V vs the reference electrode potential (red line). In this case, an anodic current is flowing and thus the potential drop is of the opposite sign. In the compensated resistance case (red curve), the value of ~ -0.100V can be understood by noting in the region just outside the EDL to the reference electrode, ϕ increases by ~ 0.051 V, resulting in the desired potential difference ($\approx$ -0.150 V).

When using 95% compensation (as in Fig. 5b and Fig. S8a) at 1000 V/s, ΔE_p is ~ 66 mV which is slightly greater than the value expected in the diffusion-only case (~ 59 mV, see section SI 3). This difference is mostly due to the remaining 5% of the resistance that is not compensated. We see this in Fig. S9, which shows voltammetry with different values of f. Decreasing f to 0.90 (= 90%) (Fig. S9a) increases ΔE_p to 76 mV while increasing to 0.99 (= 99%) leads to ΔE_p ~ 59 mV (Fig. S9c), which is equal to the diffusion model at 1000 V/s. However, other differences in the voltammetry are also apparent: the time constant decay, observed at the start of the scan and at the switching potentials, see Fig. 9d, is slower if 90% compensation (red) is applied compared to the 95% compensation (black). At 99% compensation (blue), the time-constant delay is even shorter, however, there are undesirable oscillating features near the switching potentials. This behaviour is known as "ringing" and is also seen experimentally when high values of f are employed.[7] This sign of instability in the feedback loop is known as "overcompensation" and is the reason why 100% of the ohmic potential drop cannot be compensated.
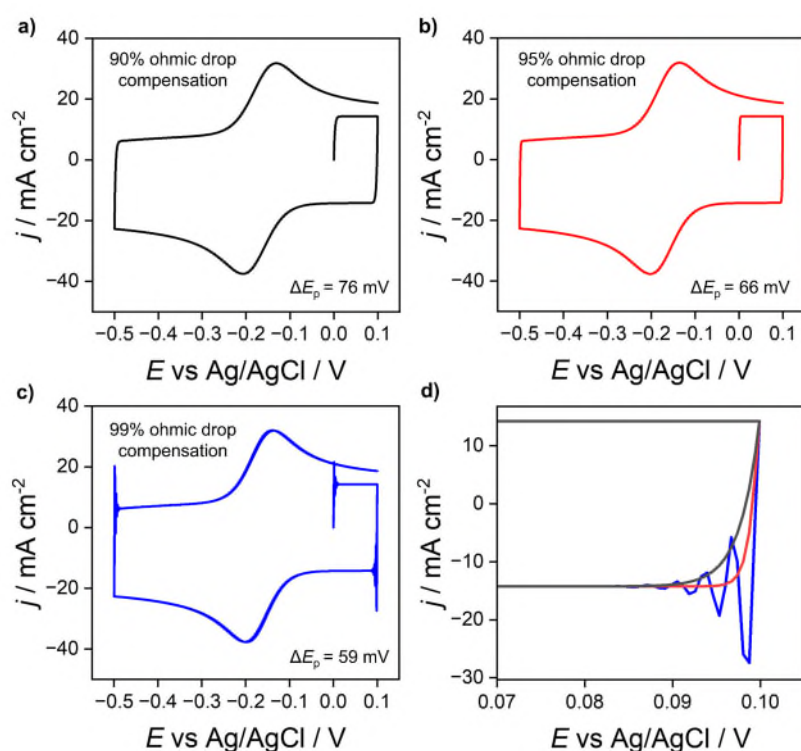

Fig. S9 *Simulated voltammograms with a) 90% b) 95% and c) 99% ohmic drop compensation at a scan rate of 1000 V/s using a gain setting of 1×10^8 as described in SI 6. d) zoomed in section at the positive switching potential corresponding to 90% (black), 95%, (red) and 99% (blue) ohmic drop compensation. All other parameters are as listed in the caption to Fig. S4.*

SI 7. Influence of the Charge of the Redox Species (*z/z*-1) on the Voltammetric Response

When the electrostatic model is applied to a system which has fast electron transfer kinetics (e.g. k^0 = 13.5 cm/s), the voltammetric response is independent of the EDL structure and the charge on the redox species, *z* and *z*-1, for O and R, respectively. As discussed in the main article (section *Why does the EDL Have No Effect on the CV response of Reversible Redox Couples?*) this is due to an equilibrium existing between the concentration of the redox species at the PET and in solution just outside the EDL, which is maintained at the scan rates in this work. However, the local concentration of the redox species is dependent on the sign and magnitude of the redox species charge. Fig. S10 shows the concentration of the O (solid) and R (dashed) species adjacent to the electrode surface for differently charged redox pairs on the (i) ~ μm scale of the diffuse layer and the (ii) ~ nm scale of the EDL at (a) *E* = +0.1 V, (b) *E* = -0.1 V, (c) *E* = $E^{0'}$ = -0.173 V and (d) *E* = -0.3 V; *v* = 1 V/s. The EDL is on the order of ~3 nm, outside of this the concentration distribution is not dependent on the charge of the redox species as can be seen on the ~ μm length scale. In contrast on the ~ nm length scales the concentration is dependent on the charge of the redox species. For example, Fig. S10 aii shows that at *E* = 0.1 V there is an accumulation of the negatively charged O^{2-} (solid green) species at the electrode surface but a depletion of O^{3+} (solid black), which is due to anion accumulation/cation depletion in the EDL, to balance the positive charge on the electrode. The opposite is true at negative potentials (parts b-d).
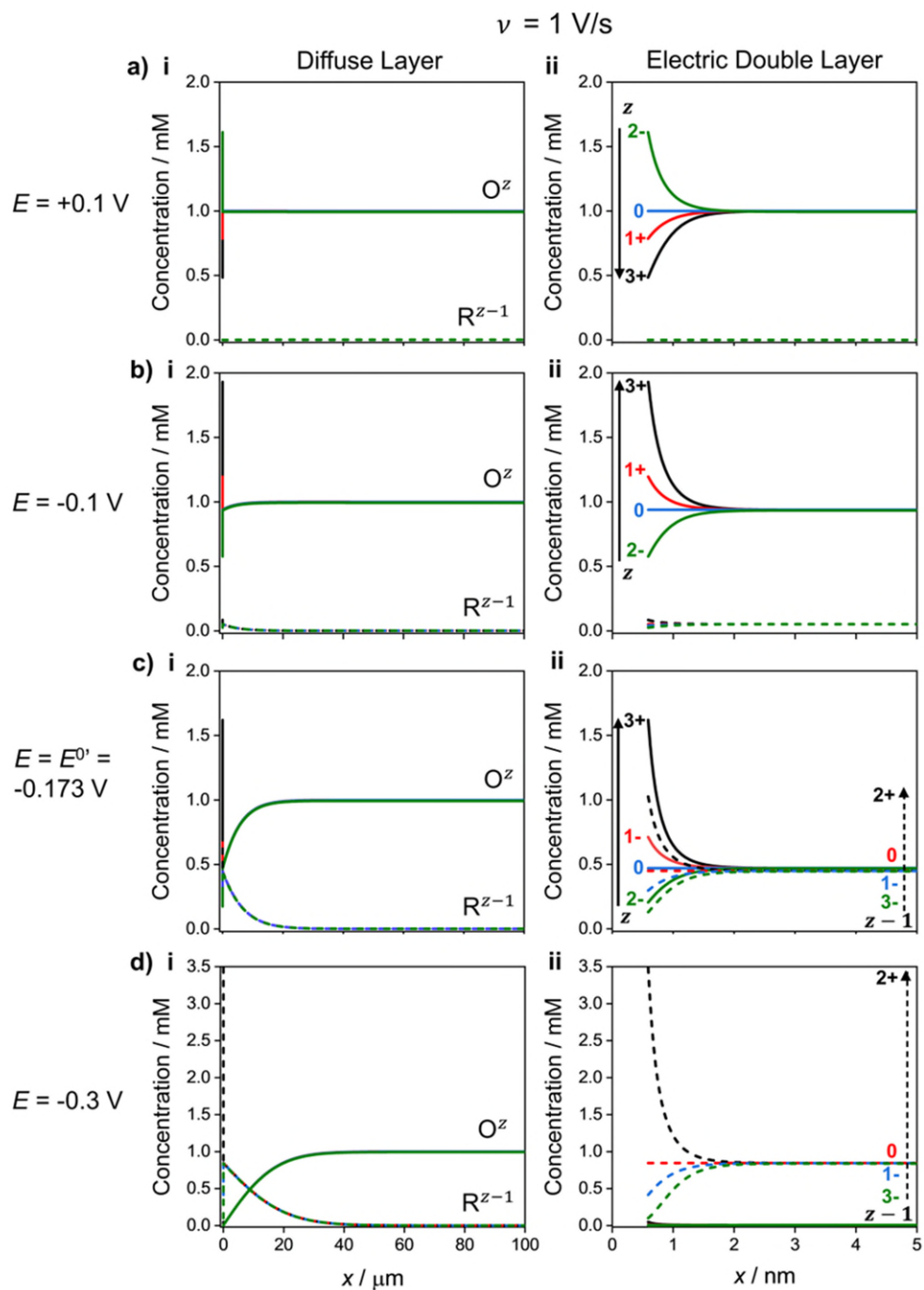
Fig. S10 *Simulated concentration distribution across solution of O^z dashed) and R^{z-1} (solid) redox species for a 1e outer-sphere redox process with varying charges (z/z-1). The charges include those of the redox couple used in this work 3+/2+ (black) in addition to +1/0 (red), 0/-1 (blue) and -2/-3 (green). The concentration distributions are reported on the cathodic scan at potential values a) E = 0.1 V b) E = -0.1 V, c) E = $E^{0'}$ = -0.173 V and d) E = -0.3 V at 1 V/s. Note: part d is on a different scale. All other parameters are as listed in the caption of Fig. S4.*

SI 8. References

1   Y. Wang, J. G. Limon-Petersen and R. G. Compton, *J. Electroanal. Chem.*, 2011, **652**, 13–17.

2   A. J. Bard, L. R. Faulkner and H. S. White, *Electrochemical Methods: Fundamentals and Applications*, Wiley, 3rd edn., 2022.

3   C. G. Malmberg and A. A. Maryott, in *J. Res. Natl. Bur. Stand.*, 1956, **56**, 1- 8.

4   A. Hamelin, T. Vitanov, E. Sevastyanov and A. Popov, *J. Electroanal. Chem. Interfacial Electrochem.*, 1983, **145**, 225–264.

5   Y. Sun, Y. Liu, Z. Liang, L. Xiong, A. Wang and S. Chen, *J. Phys. Chem. C*, 2009, **113**, 9878–9883.

6   J. Velmurugan, P. Sun and M. V. Mirkin, *J. Phys. Chem. C*, 2008, **113**, 459–464.

7   C. Amatore, E. Maisonhaute and G. Simonneau, *J. Electroanal. Chem.*, 2000, **486**, 141–155.